Universal behavior of the electron *g* factor in GaAs/$Al_xGa_{1-x}As$ quantum wells

I. A. Yugova,[1,2,*] A. Greilich,[1] D. R. Yakovlev,[1,3] A. A. Kiselev,[4] M. Bayer,[1] V. V. Petrov,[2] Yu. K. Dolgikh,[2] D. Reuter,[5] and A. D. Wieck[5]

[1]*Experimentelle Physik II, Universität Dortmund, 44221 Dortmund, Germany*

[2]*Institute of Physics, St.-Petersburg State University, St.-Petersburg 198504, Russia*

[3]*A. F. Ioffe Physico-Technical Institute, Russian Academy of Sciences, 194021 St. Petersburg, Russia*

[4]*Department of Electrical and Computer Engineering, North Carolina State University, Raleigh, North Carolina 27695-7911, USA*

[5]*Angewandte Festkörperphysik, Ruhr-Universität Bochum, D-44780 Bochum, Germany*

(Received 28 September 2006; revised manuscript received 9 April 2007; published 5 June 2007)

The Zeeman splitting and the underlying *g* factor for conduction-band electrons in GaAs/$Al_xGa_{1-x}As$ quantum wells have been measured by spin-beat spectroscopy based on a time-resolved Kerr rotation technique. The experimental data are plotted as functions of the lowest band-to-band optical transition energy, i.e., the effective band gap of the quantum wells. The model calculations suggest that in the tracked range of transition energies *E* from 1.52 to 2.0 eV, the component of electron *g* factor along the growth axis follows closely the universal dependence $g_{\parallel}(E) \approx 0.445 + 3.38(E-1.519) - 2.21(E-1.519)^2$ (with *E* given in eV), and this universality also embraces $Al_xGa_{1-x}As$ alloys. On the other hand, the in-plane *g* factor component deviates in a systematic way from this universal curve, with the degree of deviation controlled by the structural anisotropy. The experimental data are in good agreement with the theoretical predictions.

DOI: 10.1103/PhysRevB.75.245302 PACS number(s): 78.47.+p, 75.75.+a, 73.21.Fg

I. INTRODUCTION

The Lande or *g* factor of carriers in a solid is one of the fundamental material properties.[1–3] For conduction-band electrons in semiconductors and semiconductor heterostructures, it may deviate strongly from the free-electron *g* factor in vacuum, $g_0 = +2.0023$, due to the spin-orbit interaction, e.g., it is −0.44 in GaAs, −1.64 in CdTe, and can be as large as −51 in the narrow-band-gap semiconductor InSb.[5]

The invention of spintronics has increased the interest in spin manipulation in semiconductor heterostructures[2,4] and therefore in control of the carrier *g* factors. GaAs/$Al_xGa_{1-x}As$ heterostructures are very suitable for this purpose as with increasing carrier confinement the electron *g* factor's value decreases and even crosses zero. Therefore, the Zeeman splitting can be fully suppressed by a proper choice of structure design parameters and/or external conditions such as strain, temperature, electric field, and orientation of the structure in an external magnetic field.[6–8]

The electron *g* factor in GaAs/$Al_xGa_{1-x}As$ quantum well (QW) structures has been measured by various experimental techniques such as spin-flip Raman scattering,[9] optical orientation,[10–13] optically detected magnetic resonance,[14,15] and spin quantum beats in emission,[16–19] in absorption,[20] or in Kerr rotation.[21,22] However, most of these studies have been limited to certain widths of the quantum wells and only in a few papers the well width dependence of the *g* factor has been reported.[10,17,19,22]

The first concise analysis of the electron *g* factor in QWs was performed in the frame of the Kane model,[23] followed by more detailed considerations.[24–27] These model calculations predict a strong variation of the *g* factor value, including a sign reversal in the GaAs/$Al_xGa_{1-x}As$ heterosystem, and of its anisotropy with well width. Both quantities are controlled by the strength of electron confinement in the QWs determined mostly by the well width and barrier height. These theoretical predictions were further substantiated by experimental data.[19,22,28,29] The published results are commonly presented as a dependence of the *g* factor value on the QW width, i.e., a set of different dependencies corresponding to different barrier heights (controlled by the Al content) is required to cover the whole range of possible QW structures. In CdTe/$Cd_{1-x}Mg_xTe$ heterostructures, whose band structure is similar to that of GaAs/$Al_xGa_{1-x}As$ structures, to a good approximation, a *universal* dependence of the electron *g* factor on the heterostructure band gap [i.e., on the energy of the optical transition between the ground states of confined electrons (e1) and holes (hh1)] has been reported:[30] the *g* factor was sensitive mostly to the value of the band gap itself, but not to the way how this gap has been obtained by the structure's design parameters.

The goal of this paper is to check experimentally and theoretically whether this universality can be extended to GaAs/$Al_xGa_{1-x}As$ heterosystems, and if yes, what the origins of this universality are. We present experimental results for time-resolved pump-probe Kerr rotation, which allow us to determine the transverse ($g_\perp$) and longitudinal ($g_\parallel$) components of the electron *g* factor with high accuracy from the frequencies of the spin precession in an external magnetic field. Model calculations accounting for the $\boldsymbol{k}\cdot\boldsymbol{p}$ interaction between the lowest conduction band and the upper valence bands have been performed for both components of the electron *g* factor in structures with the Al content varied from 0 to 0.45. The experimental data are found to be in good agreement with the model predictions showing that some universality can be claimed for the GaAs/$Al_xGa_{1-x}As$ heterosystem.

II. EXPERIMENTAL DETAILS

The GaAs/$Al_xGa_{1-x}As$ heterostructures have been grown by molecular-beam epitaxy on (100) oriented GaAs sub-

TABLE I. Parameters of the studied GaAs/$Al_xGa_{1-x}As$ QW structures.

Sample, Al content	QW width (nm)	Transition	Laser energy (eV)	$\lvert g_\perp \rvert$	$\lvert g_\parallel \rvert$
1 (p343), x=0.33	16.0	e1-hh1	1.528	0.36±0.01	0.43±0.01
	14.3	e1-hh1	1.530	0.34±0.01	
	11.0	e1-hh1	1.540	0.30±0.01	0.43±0.01
	10.2	e1-hh1	1.543	0.27±0.01	
	7.6	e1-hh1	1.565	0.15±0.01	0.22±0.01
	7.3	e1-hh1	1.569	0.13±0.01	
	4.3	e1-hh1	1.618	0.10±0.01	0.025±0.02
	4.2	e1-hh1	1.622	0.06±0.004	
2 (p340), x=0.34	17.2	e1-hh1	1.527	0.40±0.01	
	13.0	e1-hh1	1.535	0.33±0.01	
	13.0	e1-hh1	1.542	0.33±0.01	
	13.0	e2-hh2	1.597	0.32±0.01	
	11.7	e1-hh1	1.538	0.30±0.01	0.40±0.01
	8.8	e1-hh1	1.555	0.20±0.005	
	7.9	e1-hh1	1.562	0.16±0.01	0.25±0.01
	5.1	e1-hh1	1.600	0.00±0.04	
3 (p337), x=0.28	10.0	e1-hh1	1.544	0.26±0.005	
4 (11302), x=0.25	8.4	e1-hh1	1.559	0.17±0.01	
	GaAs buffer		1.559	0.43±0.005	
5 (e294), x=0.32	8.8	e1-hh1	1.555	0.21±0.01	
	GaAs buffer		1.515	0.44±0.001	
	GaAs buffer		1.529	0.44±0.001	
	GaAs buffer		1.543	0.43±0.006	
	GaAs buffer		1.553	0.42±0.004	

strates. The sample parameters are collected in Table I. Samples 1 and 2 consist of several single QWs of different widths (four QWs in each sample) separated by 50-nm-thick $Al_xGa_{1-x}As$ barriers to prevent electronic coupling between the wells. These samples have been grown without rotation and therefore have gradients in QW widths. This is the reason for giving more than four values of g factors and corresponding QW widths and energies for a particular sample in Table I. The values which differ only slightly from one another have been recorded on the same QW but at different lateral positions. Samples 3, 4, and 5 contain only one QW. All structures are nominally undoped, but due to residual doping of the barriers, presence of background electrons in the QWs has been established from the observation of emission by negatively charged excitons. The background electron density does not exceed 5×10^9 cm^{-2}.

For optical measurements, the samples were immersed in pumped liquid helium at a temperature of 1.6 K. The structures were characterized by means of photoluminescence excited by 532 nm laser light with an excitation density below 0.3 W/cm^2. Magnetic fields up to 7 T could be applied, which, in most experiments, were oriented perpendicular to the structure growth axis (Voigt geometry). To determine the longitudinal component of the electron g factor, the magnetic field was applied obliquely to the structure growth axis. The tilt angle was 45°.

The electron g factor was evaluated from the frequency of the electron-spin quantum beats corresponding to the Larmor precession frequency in magnetic field. A pump-probe technique with polarization sensitivity based on time-resolved Kerr rotation was used for detection of the spin beats (see, e.g., Refs. 2 and 31). A Ti:sapphire laser emitting 1.8 ps pulses at a repetition rate of 75.6 MHz was tuned in resonance with the QW exciton transition. The pump beam was circularly polarized by means of an elasto-optical modulator operating at 50 kHz. The excitation density was kept as low as possible in the range from 0.2 to 1 W/cm^2. The probe beam was linearly polarized, and its intensity was about 20% of the pump beam. The rotation angle of the linear polarization plane of the probe pulse, reflected from the sample due to the Kerr rotation, was detected by a balanced diode detector and a lock-in amplifier. The time-resolved Kerr rotation signal as function of the delay between probe and pump pulses gives the evolution of the electron-spin coherence generated by the pump.

III. EXPERIMENTAL RESULTS

A typical photoluminescence spectrum obtained for sample 2 containing four single QWs of different thicknesses is shown in Fig. 1. The emission from the GaAs buffer layer

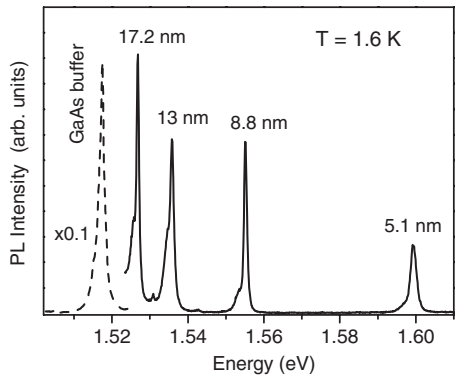

FIG. 1. Photoluminescence spectrum of a $GaAs/Al_{0.34}Ga_{0.66}As$ structure containing four single QWs of different widths (sample 2). The emission from the GaAs buffer layer is shown by the dashed line.

is presented by the dashed line. The luminescence from the QWs is dominated by recombination of excitons, whose energy increases for the narrow QWs due to confinement. The low-energy shoulders of the excitonic lines are due to the negatively charged exciton (trion) recombination.[32] The trion consisting of two electrons and a hole is formed by a background electron and a photogenerated exciton.

An example of time-resolved spin quantum beats in a 10-nm-wide QW detected in a magnetic field of $B=1$ T (Voigt geometry) is shown in Fig. 2. The experimental data are plotted by the black line. The excitation energy of 1.544 eV is resonant with the exciton transition. The periodic oscillations of the Kerr signal are due to the precession of coherently excited electron spins about the magnetic field, with the oscillation period T_L given by the spin splitting in the conduction band ΔE. Therefore, the Larmor precession frequency $\omega_L=2\pi/T_L$ allows precise determination of the transverse component of the electron g factor $g_\perp$ by

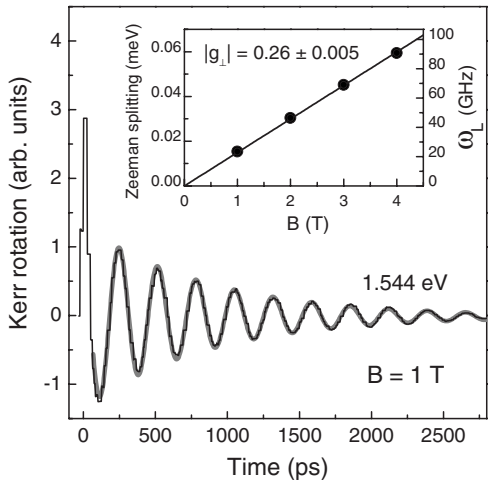

FIG. 2. Time-resolved Kerr rotation for a 10 nm QW (sample 3) in a magnetic field of 1 T. The black line gives the experimental data, and the thick gray line is a fit to the data after Eq. (2) using the parameters $\omega_L=23.4$ GHz and $\tau=880$ ps. The inset shows the Zeeman splitting ΔE (left scale) and the frequency of spin beats ω_L (right scale) as function of magnetic field. $T=1.6$ K.

$$\Delta E = \mu_B g_\perp B = \hbar \omega_L, \tag{1}$$

where μ_B is the Bohr magneton (note that the sign of the g factor cannot be determined, but only its absolute value). We fit the experimental spin-beat dynamics by a form for an exponentially damped oscillation. In case of a single frequency and a single decay time, which gives an appropriate description for most of the studied structures, this form is given by the following equation:

$$y(t) = A \exp(-t/\tau)\cos(\omega_L t), \tag{2}$$

with an amplitude A. τ is the decay time of spin coherence, which, for an electron-spin ensemble, corresponds to the spin dephasing time T_2^* (Refs. 2 and 33). An example for the result of a fitting to the experiment is given in Fig. 2 by the thick gray line. Here, we exclude from the analysis the initial 15–30 ps after the pump pulse, which are contributed by the fast relaxation of holes.[18,34,35]

In the inset, the determined Zeeman splitting is plotted as a function of magnetic field. The corresponding values of the Larmor frequency are also given on the right vertical axis. The slope of the B linear dependence gives $|g_\perp| = 0.26 \pm 0.005$. The decay time of the spin beats in Fig. 2 is 880 ps and is considerably longer than the radiative decay of resonantly excited excitons which does not exceed 100 ps in $GaAs/Al_xGa_{1-x}As$ QWs.[36] Therefore, we conclude that the detected spin beats are provided by background electrons whose spin coherence is photogenerated by the trion formation.[33] It is beyond the scope of this paper to discuss the mechanism of optical generation of spin coherency for the electron gas of low density. We only note here that the trion formation plays a key role in this process and direct readers to related studies.[33,37]

Not in all cases the Kerr signals can be described by a single frequency and/or single decay time. Figure 3 illustrates a more complicated case observed in sample 5 for an 8.8-nm-wide QW. The excitation energy of 1.515 eV is resonant with the exciton transition of the GaAs buffer layer, and the observed oscillations with $|g_\perp|=0.44$ are in accord with the known g-factor value of bulk GaAs, $g(\mathrm{GaAs})=-0.44$ (Ref. 5). The decay of the spin beats shows two characteristic times. The fast one, of 360 ps, may be associated with the exciton lifetime and the long one, which exceeds 3 ns, describes the dephasing of the background electrons in the buffer layer.[38] The resonant excitation into the exciton states of GaAs results in the largest amplitude of the Kerr signal. However, pronounced spin beats can be observed also when the excitation energy is detuned from the resonance condition and shifted further up by 14 and 27 meV to energies of 1.529 and 1.543 eV, respectively, which are still below any QW resonance. The Kerr signal at these energies is provided by the exciton-polariton reflection spectrum,[39] which is governed by the quantization of polaritons in the GaAs buffer layer. The spin-beat period is independent of the excitation energy, as it is determined by spin oriented carriers, which relax from the excited states to the bottom of the conduction band and precess there with $|g_\perp|=0.44$. The amplitude of the Kerr signal, however, decreases, as shown by the open circles in the inset.

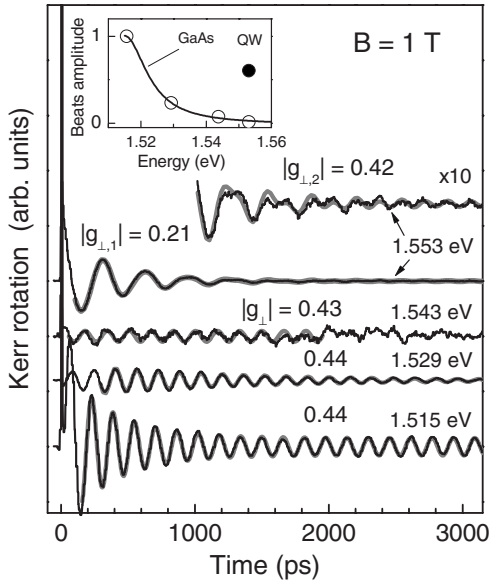

FIG. 3. Time-resolved Kerr rotation of an 8.8 nm QW (sample 5) measured at different excitation energies. The upper curve (1.533 eV) has been scaled up to clearly show the beats from the GaAs buffer layer superimposed by the QW signal. The experimental data are shown by the narrow black lines, and fit results using the forms discussed in the text are given by the thick gray lines. Inset: Relative intensities of the beats from the QW (closed circles) and the GaAs buffer layer (open circles) as function of excitation energy. $T=1.6$ K.

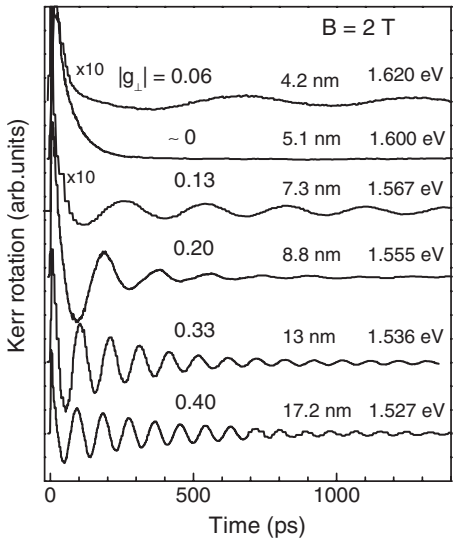

FIG. 4. Time-resolved Kerr rotation in QWs of different thicknesses (samples 1 and 2) measured in a magnetic field of 2 T. Well width, excitation energy, and g factor value are indicated at each trace. $T=1.6$ K.

An increase of the laser energy to 1.553 eV brings it in resonance with the QW exciton. The beat period increases about twice corresponding to $|g_{\perp,1}|=0.21$. The spin beats are damped with a decay time $\tau=410$ ps. At longer delays exceeding 1000 ps, the oscillation picture becomes irregular, suggesting that at least two periodic processes overlap. The signal was fitted by an equation accounting for two frequencies with different decay times:

$$y(t) = A_1 \exp(-t/\tau_1)\cos(\omega_{L,1}t) + A_2 \exp(-t/\tau_2)\cos(\omega_{L,2}t). \tag{3}$$

As one can see from the fit in Fig. 3 shown by the gray line, the experiment can be described by spin beats of QW electrons with $|g_{\perp,1}|=0.21$ superimposed with $|g_{\perp,2}|=0.42$ beats. The latter beats can be attributed to electrons precessing in the GaAs buffer. The relative intensities of the amplitudes A_1 and A_2 are given in the inset of Fig. 3 by closed and open circles, respectively.

To obtain further insight, a 13-nm-wide QW in sample 2 has been excited resonantly into three optical transitions corresponding to the ground state of the heavy-hole exciton (e1-hh1) and of the light-hole exciton (e1-lh1), as well as of the exciton related to the second confined electron and heavy-hole levels (e2-hh2). For all cases, spin beats with almost the same period corresponding to $|g_\perp|=0.33$ have been found (see Table I). As the value of the electron g factor should strongly depend on the electron energy, we therefore conclude that the Kerr signal is provided by electrons which relax to the bottom of the conduction band shortly after photogeneration and precess there. That the e1 electron precession can be accessed through the e2-hh2 optical transition is remarkable.

After having given some insight into the general features of the experimental data and their analysis, we turn to the problem of the g factor dependence on the carrier confinement conditions. Time-resolved Kerr rotation signals detected with the laser energy resonant to the exciton optical transitions in QWs of different widths are shown in Fig. 4. One can see that the spin-beat frequency, which is proportional to $|g_\perp|$ of the conduction-band electrons, decreases with decreasing well width. Oscillations cannot be resolved in a 5.1 nm QW with the exciton energy at 1.600 eV. A further decrease of the QW width down to 4.2 nm restores the spin-beat oscillations. The determined $|g_\perp|$ values are given in the figure and are collected also in Table I.

The experimental values for $|g_\perp|$ are plotted in Fig. 5 as function of resonant excitation energy. We note here that in our experiments, the sign of the electron g factor has not been measured. To plot the values, the negative sign for the wide QWs has been chosen to be in accord with the electron g factor in bulk GaAs $g(\mathrm{GaAs})=-0.44$. Most of the data, except for some results for a 13 nm QW and the GaAs buffer which were measured for nonresonant excitation, were detected when the laser was resonant with the exciton state e1-hh1. Measurements on different structures confirm the monotonic decrease of the g factor absolute value with increasing energy, leading to a sign reversal at 1.600 eV. Our results are in good agreement with the data of Snelling *et al.*[10] obtained by the optical orientation technique. They are also in good agreement with model calculations for Al contents of $x=0.3$ and 0.35 shown by the solid and the dashed lines, respectively. Details of these calculations are given below in Sec. IV. We note that the calculated dependencies are plotted as function of energy of the optical transition between the confined carrier levels e1 and hh1 without ac-

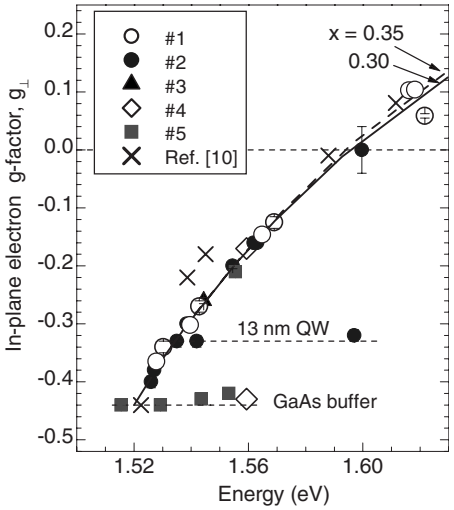

FIG. 5. Dependence of the transverse component of the electron g factor on resonant excitation energy. Symbols are experimental data for which values are taken from Table I and sign is selected based on known data for bulk GaAs, $g(\mathrm{GaAs})=-0.44$. Solid and dashed lines are calculations for Al contents of $x=0.3$ and 0.35, respectively. Horizontal dashed lines are guides to the eye $T=1.6$ K.

counting for the exciton binding energy. The latter may shift these curves to lower energy by about 8 meV in QWs of about 20 nm width and by about 13 meV in 4 nm QWs.[40]

To measure the longitudinal component of the electron g factor, we have performed time-resolved Kerr rotation experiments with magnetic field tilted relative to the heterostructure growth direction. The tilt angle Θ between the magnetic field and growth direction was 45°. An example of time-resolved spin quantum beats in an 11-nm-wide QW (sample 1) is shown by the thin black line in Fig. 6(a). A fit by Eq. (2), which is shown by the thick gray line, allows us to obtain the quantum beat frequency and evaluate the longitudinal component of the electron g factor $|g_\parallel|$ using the following equation for the Larmor frequency of electron-spin beats in tilted magnetic fields:

$$\omega_L = \mu_B B \sqrt{(g_\parallel \cos\Theta)^2 + (g_\perp \sin\Theta)^2}/\hbar. \qquad (4)$$

The measured values of $|g_\parallel|$ for samples 1 and 2 are collected in Table I. After resolving the sign ambiguity, $g_\parallel$ is also shown by the circles in Fig. 6(b) together with the results of model calculations for an Al content $x=0.3$ for $g_\parallel$ and $g_\perp$ given by the solid and dashed lines, respectively. The measured values are in reasonable agreement with the modeled dependencies, but the data scattering is obviously more prominent here and correspondence with theory is not as striking as it was for the $g_\perp$ in Fig. 5. In particular, one can see that the differences between experimental and theoretical values for $g_\parallel$ are larger for thinner QWs.

IV. CALCULATION OF THE ELECTRONIC g FACTOR AND COMPARISON WITH EXPERIMENT

Here, we present results of model calculations for the longitudinal and transverse components of the electronic g factor in $\mathrm{GaAs/Al_xGa_{1-x}As}$ QWs for a wide range of well widths from 1 to 30 nm and Al contents $0<x<0.45$, which control the barrier height. In Fig. 7, the calculated g factors are shown as function of the e1-hh1 optical transition energy. This provides a convenient comparison with experiment, as the g factor is addressed in dependence on an easily measurable quantity.

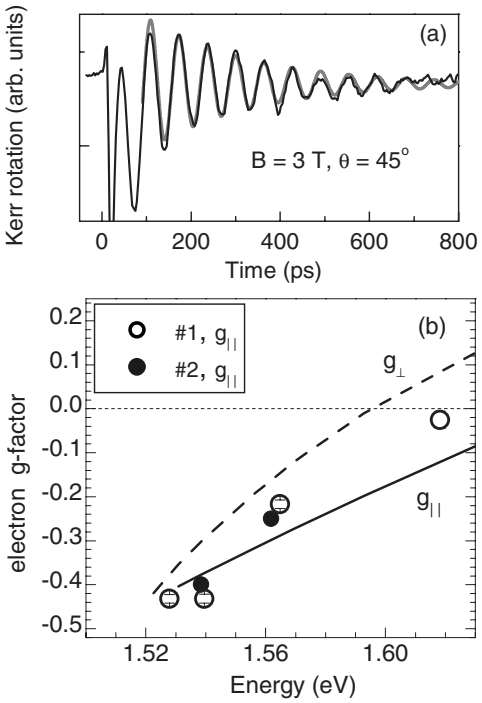

FIG. 6. (a) Time-resolved Kerr rotation for an 11 nm QW (sample 1) in a magnetic field of 3 T, $\Theta=45°$. Black line gives the experimental data, and thick gray line is a fit by Eq. (2) with the parameters $\omega_L=99$ GHz and $\tau=240$ ps. (b) Dependence of the electron g factor on resonant excitation energy. Symbols are experimental data for the longitudinal component. Solid (longitudinal component) and dashed (transverse component) lines are calculations for Al content of $x=0.3$. Horizontal dashed line shows the zero value. $T=1.6$ K.

To prepare Fig. 7, it was necessary, first, to calculate accurately the lowest quantized states of electrons and heavy holes for each set of heterostructure parameters and, second, to evaluate the g factor tensor for the calculated electron states. To achieve advanced accuracy in the energy levels, we applied the Kane multiband Hamiltonian, accounting exactly for the coupling between the lowest conduction band Γ_6 and the upper valence bands Γ_8 and Γ_7 and retaining also all remote band terms that notably affect the dispersion of the relevant quasiparticles in conduction and valence bands. Details were presented elsewhere.[41,42] Then, by directly following the prescriptions in Ref. 26, two independent components of the g factor tensor at the bottom of the first electron subband in the QW structure can be calculated: the in-plane g factor $g_\perp$ using Eq. (6) of Ref. 26 and the g factor along the growth direction $g_\parallel$ with the help of Eq. (10) of Ref. 26. For the simplest case of an unbiased, unstrained, and symmetric QW assembled from zinc-blende semiconductors, we get

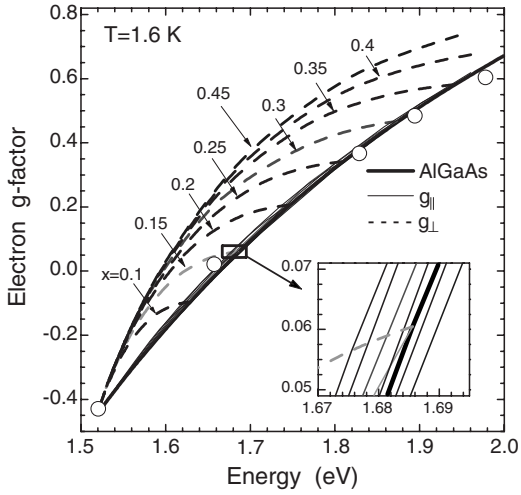

FIG. 7. Longitudinal (solid lines) and transverse (dashed lines) components of the electron g factor as function of the energy of the lowest optical transition in GaAs/$Al_xGa_{1-x}As$ QWs, calculated for various barrier compositions and different QW widths. Open circles show experimental data for bulk $Al_xGa_{1-x}As$ alloys taken from Ref. 45. Inset details the dependencies for the longitudinal g factor, which closely follow the dependence for $Al_xGa_{1-x}As$.

$$g_\perp = g_0 + \delta g_{\text{remote}} - 4\int dz D z (f^2)'_z \tag{5}$$

and

$$g_\parallel = g_0 + \delta g_{\text{remote}} + 4\int dz D[(fh)'_z + f^2]. \tag{6}$$

Here, $f(z)$ describes the spatial dependence of the conduction-band envelope function at the bottom of the electron subband in the QW and satisfies the equation

$$-\frac{\hbar^2}{m_0}\left(\frac{1}{2} + \delta\mu_{\text{remote}} + A\right) f''_{zz} + (V-E)f = 0 \tag{7}$$

and the homogeneous boundary conditions

$$f, (1/2 + \delta\mu_{\text{remote}} + A) f'_z = \text{const} \tag{8}$$

at the heterointerfaces. An auxiliary function $h(z)$ has to be obtained as solution of the same Eq. (7), but with the inhomogeneous boundary conditions involving the already found function f,

$$h, (1/2 + \delta\mu_{\text{remote}} + A) h'_z + Df = \text{const}. \tag{9}$$

Further,

$$A = \frac{P_{cv}^2}{3m_0}\left(\frac{2}{E - V + E_g} + \frac{1}{E - V + E_g + \Delta_{SO}}\right) \tag{10}$$

and

$$D = -\frac{P_{cv}^2}{3m_0}\left(\frac{1}{E - V + E_g} - \frac{1}{E - V + E_g + \Delta_{SO}}\right). \tag{11}$$

Here, m_0 is the free-electron mass in vacuum, E_g is the semiconductor band gap, P_{cv} is the interband momentum matrix element, Δ_{SO} is the spin-orbit splitting in the valence band, and $\delta\mu_{\text{remote}}$ and δg_{remote} are the remote band contributions to the conduction-electron dispersion and g factor, respectively. In a typical heterostructure, all these material parameters are piecewise constants. If in the whole structure the electron state energy E is counted, for example, from the edge of the conduction band in the well material, the piecewise constant conduction-band profile $V(z)$ should also be accounted for in Eqs. (7), (10), and (11). Lastly, the found conduction-band envelope f should be normalized to satisfy the normalization condition for the full three-band electron wave function.

TABLE II. Band-structure parameters for GaAs and $Al_{0.35}Ga_{0.65}As$. Also included is the type of interpolation procedure for the $Al_xGa_{1-x}As$ alloys. The data have been taken from Ref. 5.

	GaAs	$Al_{0.35}Ga_{0.65}As$	Interpolation
Δ_{SO} (eV)	0.341	0.32	Basic, linear
$2P_{cv}^2/m_0$ (eV)	28.9	26.7	Basic, linear for P_{cv}
m_{bulk}/m_0	0.067	0.09	Composite
g_{bulk}	−0.44	0.58	Composite
m_{hh}/m_0	0.45	0.45	Constant

Most parameters characterizing the band structure of the $Al_xGa_{1-x}As$ alloy are well established. The numerical values for all applicable quantities are collected in Table II for GaAs and $Al_{0.35}Ga_{0.65}As$ (the data have been taken from Ref. 5). The following scheme for parameter evaluation has been adopted for an arbitrary Al composition x: for most of the parameters (named *basic* in Table II), we use a simple linear interpolation (extrapolation for $x > 0.35$). This group contains P_{cv} and Δ_{SO}. Rigorously speaking, higher accuracy could probably be achieved if also the bowing constants for the interpolation curves were known, but for the studied range $0 < x < 0.45$, linear interpolations are reasonable. As the only notable exception, we use the common interpolation equation with bowing term for the $Al_xGa_{1-x}As$ band gap:[5]

$$E_g(x) = 1.519 + 1.04x + 0.47x^2\ [eV]. \tag{12}$$

Some parameters are obviously model derivatives and we denote them as *composite*: the bulk electron effective mass m_{bulk} and the bulk g factor g_{bulk} are defined by a subset of basic quantities. These composite parameters are not expected to follow a linear interpolation law, so we apply a different approach: when we need the bulk value of a composite parameter for some alloy composition, we directly *calculate* it from *interpolated* basic parameters. For example,[43]

$$g_{\text{bulk}} = g_0 - \frac{4}{3}\frac{P_{cv}^2}{m_0}\frac{\Delta_{SO}}{E_g(E_g + \Delta_{SO})} + \delta g_{\text{remote}}, \tag{13}$$

which can also be derived from Eq. (5) or (6) in the limit of a very wide QW. First, we use Eq. (13) and the specific numerical values of g_{bulk} from Table II to evaluate δg_{remote} for GaAs and $Al_{0.35}Ga_{0.65}As$. The obtained δg_{remote} is treated hereafter as basic and its value is interpolated. Now, when necessary, we apply Eq. (13) again to calculate g_{bulk} for any

alloy composition from a complete set of interpolated basic parameters. The heavy-hole effective mass m_{hh} is taken to be independent of the alloy composition. A ratio $\Delta E_C/\Delta E_V = 60/40$ for the offsets in the conduction and valence bands was taken for the calculations.[44]

Let us now describe in detail the results summarized in Fig. 7. Here, the two independent components of the g factor tensor are shown for an electron confined in QWs with different barrier compositions x as function of the e1-hh1 optical transition energy. The components for magnetic field applied parallel ($g_\parallel$) and perpendicular ($g_\perp$) to the structure growth axis are given by the solid and dashed lines, respectively. For every composition of the barrier material, $g_\perp > g_\parallel$. The lowest energy for the optical transition is achieved for an infinitely wide QW, for which the energy asymptotically approaches that of bulk GaAs (1.519 eV at $T=1.6$ K) and both g-tensor components converge to meet the electron g factor value in the bulk: $g(\mathrm{GaAs})=-0.44$. Therefore, for each x value, the curves for the two g factor components form something like a petal with its *root* corresponding to the principal band gap and the g factor of bulk GaAs and the *tip* corresponding to the values of the $Al_xGa_{1-x}As$ barriers (limit of a very narrow QW). As the band gap and the g factor both grow monotonously with the Al composition, the petal size also increases and its tip draws, obviously, the line $g_{\mathrm{bulk}}(E_g)$ corresponding to the bulk g factor value for a range of alloy compositions (shown in Fig. 7 by a thick solid line, and open circles are experimental data for $Al_xGa_{1-x}As$ alloys[45]).

The thick solid line in Fig. 7 is defined by Eq. (13): assuming linear interpolations for P_{cv}, Δ_{SO}, and $\delta g_{\mathrm{remote}}$ and the composition dependence for $E_g(x)$ given by Eq. (12), $g_{\mathrm{bulk}}(E_g)$ can easily be recovered analytically as a series expansion. For the GaAs/$Al_xGa_{1-x}As$ heterosystem, the first terms in the expansion are[5]

$$g_{\mathrm{bulk}}(E_g) \approx -0.445 + 3.38(E_g - 1.519) - 2.21(E_g - 1.519)^2, \tag{14}$$

with E_g measured in eV.

Quite remarkably, in our three-band Kane model, the growth direction component $g_\parallel(E_{\mathrm{e1\text{-}hh1}})$ follows *very closely* the $Al_xGa_{1-x}As$ bulk dependence $g_{\mathrm{bulk}}(E_g)$ for an arbitrary barrier composition. The inset in Fig. 7 shows a close-up of the energy dependence of $g_\parallel$ for different x. It illustrates that the $g_\parallel$ values for the whole range of x from 0 up to 0.45 basically coincide, besides minor deviations, with the dependence for bulk $Al_xGa_{1-x}As$.

Although $g_\perp$ follows generally the same trend, it deviates notably from the alloy dependence. This deviation is caused by the structural anisotropy in the heterostructure; therefore, it depends on the barrier height and strength of spatial confinement. However, for the studied GaAs/$Al_xGa_{1-x}As$ QWs, the maximum deviation of $g_\perp$ from the bulk dependence is always moderate and never exceeds 0.3. Also, in the immediate vicinity of the petal root (corresponding to the case of very weak spatial confinement and negligible penetration of the electron state into barriers), some universality with respect to different barrier compositions can be spotted for $g_\perp$.

V. DISCUSSION

In order to assess the meaning and the validity of the universal dependence of the g factor on the heterostructure band gap, let us first consider a hypothetical alloy heterosystem A_xB_{1-x}. We assume that the system can be accurately described by the Kane model, in which the two basic parameters, (i) the interband matrix element P_{cv} and (ii) the spin-orbit splitting of valence band Δ_{SO}, are plain independent of the composition (consequently, these quantities will be equal in the well and barrier layers). Another assumption is that (iii) the valence-band offset at the A_xB_{1-x}/A_yB_{1-y} heterointerface is exactly zero for any compositions x and y. Utilizing Eqs. (5) and (6) for such a hypothetic heterosystem, a *truly* universal dependence of the electron g factor on the e1-hh1 energy in the QW structure is directly obtained. Indeed, the energy-dependent coefficients A and D are continuous across the heterointerface and independent of the barrier composition; the "inhomogeneous" auxiliary function h vanishes exactly; and Eqs. (5) and (6) reduce to the same functional form, so no g factor anisotropy is present. We would like to note also that, independent of any of the assumptions above, some variant of weak universality shows up when the QW barriers in the heterostructures are extremely high, preventing a considerable penetration of the electron wave function into the barriers and, thus, a dependence of the g factor on barrier material parameters.

In reality, conditions (i)–(iii) are not fulfilled, so that the degree of the parameter mismatch (along with the extent of the penetration of a confined electron into the barrier layers) governs the deviations from the universal behavior when one changes barrier composition and QW width. The matrix element P_{cv} is modified only moderately from one semiconductor to another, and the modulation in the value of Δ_{SO} is almost negligible in cation-substituted materials, including the $Al_xGa_{1-x}As$ alloys. However, it can be considerable in anion-substituted solid solutions.[5] Condition (iii) appears to be most vulnerable, as the valence-band offset accounts for about 40% of the difference in band gaps for the well and barrier materials in GaAs/$Al_xGa_{1-x}As$ heterostructures. However, some approximate universality can be reasonably expected, with deviation severely limited by the strength of electron penetration into barriers and, in the worst scenario, comparable to the g tensor anisotropy $g_\perp - g_\parallel$. The profound universality revealed theoretically in the behavior of the growth direction component of the electron g factor, $|g_\parallel|$, in GaAs/$Al_xGa_{1-x}As$ QWs (even though it is not exact) obviously *exceeds* these expectations. We found that it appears due to a fragile and delicate balance in the dependence of the material parameters on composition: when the band gap increases with Al content, slight reductions of P_{cv} and Δ_{SO} *counterplay* and *mostly compensate* the indirect effect of moderate but nonzero valence-band offset for the type-I band alignment at the heterointerface; the particular value of m_{hh} also helps. The experiment seems to support these conclusions; although the measured values of $g_\parallel$ shown in Fig. 6 are in fair agreement with the modeled dependencies, the coincidence is actually far from being perfect.

In summary, the electronic g factor has been studied experimentally and theoretically in GaAs/$Al_xGa_{1-x}As$ QWs for

a wide range of well widths and Al contents. The results are presented as a g factor dependence on the energy of the e1-hh1 optical transition in QWs, which provides a convenient way for direct comparison of experimental data with the model calculations. A very good coincidence of experiment and theory is found for the g tensor transverse components $g_\perp$, and a reasonable agreement is established for the longitudinal components $g_\parallel$. With some reservations, a universal behavior of the electron g factor has been established for GaAs/$Al_xGa_{1-x}As$ QWs. More generally, these approximate universalities in the g factor behavior can be expected for cation-substituted alloy heterostructures with a type-I band alignment and small-to-moderate valence-band offsets. Heterosystems with these properties are known to include a number of important III-V and II-VI ternary semiconductors. However, one should be cautious about an indiscriminate extension of such conclusions to arbitrary materials.

ACKNOWLEDGMENTS

We appreciate fruitful discussions with E. L. Ivchenko and I. V. Ignatiev. We are thankful to R. T. Harley for providing us additional information about his samples. This work has been supported by the BMBF program "nanoQUIT," by the DFG Grant No. YA 65/5-1, by the ISTC Grant No. 2679, and by the RFBR Grant No. 06-02-17157. Research stays of I.A.Y. in Dortmund have been financed by the Deutsche Forschungsgemeinschaft via Graduiertenkolleg 726 "Materials and Concepts for Quantum Information Processing" and Grants No. 436 RUS 17/98/05 and No. 436 RUS 17/69/06. A.A.K. acknowledges partial financial support from DARPA and ONR.

*Electronic address: irina_yugova_05@mail.ru

[1] A. Abragham and B. Bleaney, *Electron Paramagnetic Resonance of Transition Ions* (Clarendon, Oxford, 1970).
[2] *Semiconductor Spintronics and Quantum Computation*, edited by D. D. Awschalom, D. Loss, and N. Samarth (Springer-Verlag, Heidelberg, 2002).
[3] H. Kosaka, A. A. Kiselev, F. A. Baron, K. W. Kim, and E. Yablonovitch, Electron. Lett. **37**, 464 (2001).
[4] I. Zutic, J. Fabian, and S. Das Sarma, Rev. Mod. Phys. **76**, 323 (2004).
[5] *Intrinsic Properties of Group IV Elements and III-V, II-VI, and I-VII Compounds*, edited by O. Madelung, Landolt-Bornstein, New Series, Group III, Vol. 22, Pt. A (Springer, Berlin, 1987); *Semiconductors: Basic Data*, edited by O. Madelung (Springer, Berlin, 1996).
[6] G. Salis, Y. Kato, K. Ensslin, D. C. Driscoll, A. C. Gossard, and D. D. Awschalom, Nature (London) **414**, 619 (2001).
[7] H. W. Jiang and E. Yablonovitch, Phys. Rev. B **64**, 041307(R) (2001).
[8] M. Oestreich and W. W. Ruhle, Phys. Rev. Lett. **74**, 2315 (1995).
[9] V. F. Sapega, M. Cardona, K. Ploog, E. L. Ivchenko, and D. N. Mirlin, Phys. Rev. B **45**, 4320 (1992).
[10] M. J. Snelling, G. P. Flinn, A. S. Plaut, R. T. Harley, A. C. Tropper, R. Eccleston, and C. C. Phillips, Phys. Rev. B **44**, 11345 (1991).
[11] E. L. Ivchenko, V. P. Kochereshko, I. N. Uraltsev, and D. R. Yakovlev, in *High Magnetic Fields in Semiconductor Physics III*, edited by G. Landwehr, Springer Series in Solid-State Science, Vol. 101 (Springer, Berlin, 1992), p. 533.
[12] V. K. Kalevich and V. L. Korenev, Pis'ma Zh. Eksp. Teor. Fiz. **56**, 257 (1992) [JETP Lett. **56**, 253 (1992)].
[13] V. K. Kalevich, B. P. Zakharchenya, and O. M. Fedorova, Fiz. Tverd. Tela (S.-Peterburg) **37**, 287 (1995) [Phys. Solid State **37**, 154 (1995)].
[14] H. W. van Kesteren, E. C. Cosman, W. A. J. A. van der Poel, and C. T. Foxon, Phys. Rev. B **41**, 5283 (1990).
[15] P. G. Baranov, L. V. Mashkov, N. G. Romanov, P. Lavallard, and R. Planel, Solid State Commun. **87**, 649 (1993).
[16] A. P. Heberle, W. W. Ruhle, and K. Ploog, Phys. Rev. Lett. **72**, 3887 (1994).
[17] R. M. Hannak, M. Oestreich, A. P. Heberle, W. W. Ruhle, and K. Kohler, Solid State Commun. **93**, 313 (1995).
[18] T. Amand, X. Marie, P. Le Jeune, M. Brousseau, D. Robart, J. Barrau, and R. Planel, Phys. Rev. Lett. **78**, 1355 (1997).
[19] P. Le Jeune, D. Robart, X. Marie, T. Amand, M. Brousseau, J. Barrau, V. Kalevich, and D. Rodichev, Semicond. Sci. Technol. **12**, 380 (1997).
[20] S. Bar-Ad and I. Bar-Joseph, Phys. Rev. Lett. **66**, 2491 (1991).
[21] A. Malinowski, M. A. Brand, and R. T. Harley, Solid State Commun. **116**, 333 (2000).
[22] A. Malinowski and R. T. Harley, Phys. Rev. B **62**, 2051 (2000).
[23] E. L. Ivchenko and A. A. Kiselev, Fiz. Tekh. Poluprovodn. (S.-Peterburg) **26**, 1471 (1992) [Sov. Phys. Semicond. **26**, 827 (1992)].
[24] E. L. Ivchenko, A. A. Kiselev, and M. Willander, Solid State Commun. **102**, 375 (1997).
[25] A. A. Kiselev, E. L. Ivchenko, and U. Rossler, Phys. Rev. B **58**, 16353 (1998).
[26] A. A. Kiselev, K. W. Kim, and E. L. Ivchenko, Phys. Status Solidi B **215**, 235 (1999).
[27] E. L. Ivchenko, *Optical Spectroscopy of Semiconductor Nanostructures* (Alpha Science International, Harrow, 2005), p. 238.
[28] A. A. Sirenko, T. Ruf, K. Eberl, M. Cardona, A. A. Kiselev, E. L. Ivchenko, and K. Ploog, *in High Magnetic Fields in Semiconductor Physics*, edited by G. Landwehr and W. Ossau (World Scientific, Singapore, 1996), p. 561.
[29] A. A. Kiselev, E. L. Ivchenko, A. A. Sirenko, T. Ruf, M. Cardona, D. R. Yakovlev, W. Ossau, A. Waag, and G. Landwehr, J. Cryst. Growth **184/185**, 831 (1998).
[30] A. A. Sirenko, T. Ruf, M. Cardona, D. R. Yakovlev, W. Ossau, A. Waag, and G. Landwehr, Phys. Rev. B **56**, 2114 (1997).
[31] S. A. Crooker, D. D. Awschalom, J. J. Baumberg, F. Flack, and N. Samarth, Phys. Rev. B **56**, 7574 (1997).
[32] H. Buhmann, L. Mansouri, J. Wang, P. H. Beton, N. Mori, L. Eaves, M. Henini, and M. Potemski, Phys. Rev. B **51**, 7969 (1995).

[33] E. A. Zhukov, D. R. Yakovlev, M. Bayer, G. Karczewski, T. Wojtowicz, and J. Kossut, Phys. Status Solidi B **243**, 878 (2006).
[34] N. Linder and L. J. Sham, Physica E (Amsterdam) **2**, 412 (1998).
[35] I. Ya. Gerlovin, Yu. K. Dolgikh, S. A. Eliseev, V. V. Ovsyankin, Yu. P. Efimov, I. V. Ignatiev, V. V. Petrov, S. Yu. Verbin, and Y. Masumoto, Phys. Rev. B **69**, 035329 (2004).
[36] G. Finkelstein, V. Umansky, I. Bar-Joseph, V. Ciulin, S. Haacke, J. D. Ganiere, and B. Deveaud, Phys. Rev. B **58**, 12637 (1998).
[37] T. A. Kennedy, A. Shabaev, M. Scheibner, Al. L. Efros, A. S. Bracker, and D. Gammon, Phys. Rev. B **73**, 045307 (2006).
[38] J. M. Kikkawa and D. D. Awschalom, Phys. Rev. Lett. **80**, 4313 (1998).
[39] A. Tredicucci, Y. Chen, F. Bassani, J. Massies, C. Deparis, and G. Neu, Phys. Rev. B **47**, 10348 (1993).
[40] D. B. Tran Thoai, R. Zimmermann, M. Grundmann, and D. Bimberg, Phys. Rev. B **42**, 5906 (1990).
[41] A. A. Kiselev, K. W. Kim, and E. Yablonovitch, Phys. Rev. B **64**, 125303 (2001).
[42] A. A. Kiselev, K. W. Kim, and E. Yablonovitch, Appl. Phys. Lett. **80**, 2857 (2002).
[43] L. M. Roth, B. Lax, and S. Zwerdling, Phys. Rev. **114**, 90 (1959).
[44] *Semiconductor Quantum Structures*, edited by C. Klingshirn, Landolt-Bornstein, New Series, Group III, Vol. 34, Pt. 1 (Springer, Berlin, 2001).
[45] C. Hermann and C. Weisbuch, Phys. Rev. B **15**, 823 (1977).